Materials and Methods

CHAPTER III

MATERIALS AND METHODS

This chapter explicate the methodology employed in the design and development of an air assisted electrostatic sprayer suitable for coconut palms. Each stage of the research work from the conceptualization to the prototype testing and evaluation are detailed, aiming to provide a comprehensive understanding of the engineering and scientific principles underlying the development of an electrostatic sprayer for coconut palms.

3.1 PALM ARCHITECTURE

Studies on the important plant parameters that influence the design process is the primary step for the development of an air-assisted nozzle with electrostatic charging system. The observations on parameters including height of palm, canopy diameter and angle of leaf orientation of 30 palms were done at Instructional Farm, KCAEFT, Tavanur (10.8412° N, 75.9938° E). All the observations were made by climbing the palms with standing type coconut tree climber. Canopy diameter was measured by measuring the length of two leaves situated opposite to each other. Angle of leaf orientation of lower most leaf was measured as we are spraying from downside. The measurements of leaf angle were done with the help of a goniometer.

3.1.1 Palm height

The height of the coconut tree was measured as the vertical distance from the base of the trunk at ground level to the point where the first leaf (frond) emerges from the crown. To measure the height, a standing-type coconut tree climber and a measuring tape were used. The climber was inspected for safety and securely fastened around the base of each palm. The operator wore a safety harness to ensure personal safety while ascending. After securely attaching the climber, the operator gradually climbed the palm. Upon reaching the desired point at the top of the tree, a flexible measuring tape was used to measure the distance from the ground to the topmost point of the palm.

The measurements were recorded carefully to ensure accuracy, and the process was repeated for each tree under study.

3.1.2 Canopy diameter

The canopy diameter of each coconut palm was measured using a measuring tape. Two points at the outer edges of the canopy were identified along the widest span and marked to ensure an accurate measurement. The distance between these two points was measured on the ground using the tape, recording this as the canopy diameter. To account for possible irregularities in canopy shape, a second measurement was taken perpendicular to the first, and the average of the two measurements was calculated to obtain a more representative canopy diameter for each palm.

3.1.3 Angle of leaf orientation

The inclination of the lowest leaves of each coconut palm was measured with respect to the vertical using a goniometer. The sucking pests especially whitefly infestation was observed to be concentrated on matured lower leaves. Hence the lowest mature leaves were selected for measurement, and a standing-type coconut tree climber was used to access them safely. The goniometer was positioned along the midrib of each leaf, with one arm aligned vertically and the other following the natural angle of the leaf, ensuring no alteration to the leaf's position. The angle displayed by the goniometer was recorded as the inclination with respect to the vertical. This process was repeated for multiple lower leaves to obtain an average inclination angle for each palm.

3.2 EXISTING SPRAYING METHODS FOR COCONUT

The spraying of agro-chemicals as well as biological control agents for pest management on coconut palms was carried out using a rocker sprayer, a widely used method for treating tall trees in the field. The rocker sprayer consists of a manual piston pump, a high-pressure hose, and a long spray lance. In the field, the process begins with the operator filling the sprayer with the diluted pesticide solution. Once the pump is activated, the operator manually pumps the handle to build up pressure in the system,

which forces the liquid through the hose and out of the nozzle at the end of the lance. The nozzle is directed at the canopy, aiming to cover the leaves and crown of the coconut palm.

The lance, which can be extended in length to certain degree, is used to reach the lower and middle parts of the tree's canopy, but it is often not sufficient to cover the full height of the tree. The spray generated by the rocker sprayer is typically a mix of coarse and fine droplets. The fine droplets, while ideal for coverage, are prone to drift, especially in windy conditions, leading to substantial loss of spray liquid and reduced efficiency. As the operator directs the nozzle toward the canopy, the spray is applied in a sweeping motion, moving from the base upward or from one side to another to ensure that the liquid reaches as much of the tree as possible.

However, due to the large volume of liquid required to effectively cover the tree, the application is often excessive, especially for the taller trees. This high-volume application not only results in wastage of pesticide by dripping, but also increases the spray drift, where fine droplets are carried by the wind to unintended areas, including nearby vegetation, soil, and water bodies. Additionally, the intermittent pumping action of foot sprayers itself creates fluctuations in pressure, leading to an inconsistent spray pattern that may also result in uneven distribution across the canopy. As a consequence, certain areas of the tree may result in over application of pesticide, while others may be inadequately treated, reducing the overall effectiveness of pest control.

Operator’s safety is also one of the major concerns, as they remain in close proximity to the spray plume, increasing their exposure to the chemicals. Without proper protective equipment, this can pose significant health risks, due to direct skin contact or inhalation of pesticide vapours. Furthermore, the large quantities of spray liquid used often lead to pesticide runoff, contaminating the surrounding soil and water bodies, posing environmental hazards to non-target organisms and habitats.

Power sprayers are another tool for coconut spraying, offering advantages such as quick coverage, high reach, and efficiency in pest and nutrient applications. Operating at pressure ranges typically between 2 to 35 bar. They save time and labour

compared to other spraying methods and are suitable for large plantations. However, they have drawbacks such as chemical drift, high fuel or energy consumption, and the need for regular maintenance. Similarly, large-scale mist blowers offer a versatile solution by combining air and pressure to produce fine mist droplets capable of reaching heights of 10 to 15 m.

3.3 ELECTROSTATIC SPRAYING SYSTEMS

Electrostatic spraying of plant protection products revolutionizes the traditional pesticide application methods by harnessing the power of electrostatics to enhance efficiency, efficacy and environmental sustainability. In the design of an electrostatic induction charging of agricultural spray droplets, the choice of electrode polarity was a critical parameter driven by a comprehensive understanding of plant surface characteristics. The plants were capable of developing a negative charge through several natural processes. As the plants are in contact with the Earth's crust, they may gain electrons from the ground and ion exchange processes between the soil environment. Furthermore, frictional interactions like wind blowing and movement of branches and leaves may lead to their negative charge. Biological activities including respiration and photosynthesis can enhance the negative charge accumulation over plant surfaces (Bowker and Crenshaw, 2007; Clarke *et al*., 2017; Lu *et al*., 2020).

The spray cloud with a positive charge exhibits an affinity towards the plants, as there is an inherent net negative charge present on plant surfaces. Thus, by employing a negative electrode, positively charged spray droplets are generated by electrostatic induction. These positively charged spray droplets have a strong affinity for negatively charged plant surfaces. This attraction facilitates unparallelled adhesion and coverage ensuring spray droplets are uniformly deposited over the target area with precision.

3.3.1 Principles of electrostatic charging of spray droplets

Electrostatic charging relies on the transfer of electrons between a high voltage source and spray droplets, governed by principles like the triboelectric effect and electrostatic induction. When a charged object comes in contact or brought near neutral

object, it includes a redistribution of electrons, resulting in one side becoming positively charged and the other becoming negatively charged.

The engineering management of tiny airborne particles can be improved by the application of electric field. The necessary prerequisite for electrical force management of particles bigger than those that can be substantially moved by dielectrophoretic forces of spatially divergent fields are given as (Law, 1978):

$$\overrightarrow{F_p} = q_p \vec{E} \qquad \text{Equation 1}$$

Where,

$\overrightarrow{F_p}$: Electrical force experienced by individual particle, N

q_p : Net unipolar charge, C

$\vec{E}$: Electrical potential gradient at the point of particle formation, $V \cdot m^{-1}$

The deficiency or surplus of electron makes the spray liquid to either positive or negative. The charge imparted to the droplets depends on charging capacity of the system influenced by electrode potential and spray parameters (Matthews, 1989; Appah *et al.*, 2019; Khatawkar *et al.*, 2024).

3.3.2 Droplets in electric field

An isolated charged droplet of radius 'r' consists of two types of energy: surface tension (σ) and the charge on the surface (q). The Coulomb repulsion due to the presence of net electric charge on the surface of the droplet reduces the binding force that holds the droplet together. When the electrostatic force overcomes the surface tension, the droplet breaks. This unstable condition is termed as *Coulombic fission*. The first theoretical study on this was conducted by Rayleigh. He determined that the Coulomb fission may occur, when the net charge, q on the droplet surface attains a limiting value, called Rayleigh limit, given as (Taylor, 1964; Gomez and Tang, 1994; Zheng *et al.,* 2002; Gu *et al.,* 2007; Singh *et al.*, 2013):

$$q_{max} = 8\pi\sqrt{\gamma\varepsilon_0 r^3} \qquad \text{Equation 2}$$

Where,

q_{max} : Charge on the droplet
γ : Surface tension
ε_0 : Permittivity of air (constant)
r : Droplet radius

The properties of a reliable electrostatic spraying system are nozzle type, nozzle spacing, angle, applied voltage, flow rate, pressure, spraying distance or height, electrode distance, electrode position and size. These parameters should be optimised to ensure maximum chargeability and effective spray droplet deposition. Moreover, the induced electrostatic force helps the charged droplets to levitate in air against the gravitational force (Patel, 2016; Appah *et al.,* 2019).

3.3.3 Charge acquisition methods

Among the three different electrostatic charging methods, electrostatic induction charging with an embedded electrode was chosen for this study, as it is a non-contact and safe charging method. This method also offers efficient energy transfer over short distances, which make them suitable for compact and portable devices with minimum risk of electric shock and easiness in construction (Law, 1978; Khatawkar *et al*., 2021). Furthermore, electrostatic induction charging has advantages such as, reduced operating voltage for a given charge, as the charging occurs from zero field strength upwards; easier electrode insulation as the electric field strength is lower than the air breakdown strength; lesser current capacity required for the power supply as the theoretical current requirement is zero (Marchant and Green, 1982; Zhao *et al.*, 2005).

The theoretical criteria for inducing electric charge on spray droplets by the electrostatic induction process were significantly influenced by the rate at which charges are transferred to the droplet formation zone in relation to the time required for

droplet formation. The time constant, expressed in terms of the liquid's dielectric constant (κ), air permittivity (ε_0), and resistivity (ϱ) is given as:

$$\tau = \kappa \times \varepsilon_0 \times \varrho \qquad \text{Equation 3}$$

Where τ is the time constant or charge-relaxation time in seconds. The objective of this study to impart unipolar charge to water-based solutions with electrical resistivity (ϱ) in the range of 2 to 200 Ω·m, and dielectric constant (κ) of 78.4 at 30ºC.

$$\tau = 78.4 \times 8.85 \times 10^{-12} \times 200 = 1387.68 \times 10^{-10} \text{ s}$$

(Permittivity of air = 8.85×10^{-12} $C^2 \cdot N^{-1} \cdot m^{-2}$)

The electrostatic-induction charging procedure should theoretically work with spray liquids whose charge-transfer time constants is smaller than the length of time (t_f) that characterizes the droplet formation ($\tau < t_f$). Whereas the liquids whose charge-transfer time constants are higher than the length of time ($\tau > t_f$) could not be properly charged by this method. The equation for length of time (t_f) in seconds is given as (Law, 1978):

$$t_f = \frac{l_c}{v} \qquad \text{Equation 4}$$

Where l_c is the horizontal length of liquid sheet cylindroid in meter and v is the flow velocity in $m \cdot s^{-1}$. The value of l_c was observed as 1.1 cm. The discharge (Q) of nozzle orifice with 0.5 mm diameter aperture at an operating pressure of 5 $kg \cdot cm^{-2}$ pump was found to be 2.08 $mL \cdot s^{-1}$. From discharge using the continuity equation the velocity of flow was calculated as 10.60 $m \cdot s^{-1}$. Hence, length of time (t_f) was computed as:

$$t_f = \frac{1.1 \times 10^{-2}}{10.59} = 1.038 \times 10^{-3}\ s$$

Since τ << t_f the vital theoretical requirement for electrostatic charging by induction of spray liquids was fulfilled.

3.3.4 Spray cloud current and charging efficiency of electrostatic induction charger

The electrostatic-induction charger model for τ << t_f can be theoretically modelled by two coaxial conducting cylinders which can predict the total droplet current, the surface charge density of the liquid jet, and the electric-field strength at the droplet-formation zone. Based on the field equation for concentric conducting cylinders of infinite length, the electric-field intensity (E_j) just off the surface of the liquid jet of radius, r_c (m) was approximately given as a function of applied potential difference, V (V) and radius of outer cylinder i.e. the radius of charging electrode r_e (m). The mathematical equation for electric-field intensity (E_j) was given as (Attwood, 1932),

$$E_j = \frac{V}{r_c \ln\left(r_e / r_c\right)},\ V \cdot m^{-1} \qquad \text{Equation 5}$$

According to Gauss' law, the free surface charge density, ρ_s (C·m^{-2}) on the liquid sheet cylindroid will be,

$$\rho_s = \varepsilon_0 \times E_j,\ C \cdot m^{-2}$$

As a result, the charged liquid's expected spray-cloud current, i_c (A) would be,

$$i_c = 2\pi r_c \times \rho_s \times V,\ C \cdot m^{-2}$$

The above spray-cloud current prediction equation can be expressed in terms of applied electric voltage, V (V) and liquid flow velocity, v (m·s^{-1}) as,

$$i_c = \frac{2\pi\varepsilon_0 V v}{\ln\left(r_e/r_c\right)},\ A \qquad \text{Equation 6}$$

From the observed value of Volume Mean Diameter (VMD) or D_{v50}, the theoretical droplet charge, q_p (C) can be predicted as,

$$q_p = \frac{30\varepsilon_0 r_p V}{\ln\left(2r_e/r_p\right)},\ C \qquad \text{Equation 7}$$

Where r_p is the particle radius or radius of the droplet.

The volume and mass of the spherical droplets can be calculated from the value of VMD or D_{v50} as,

$$V_{Dv50} = \frac{4}{3}\pi {r_p}^3,\ \text{m}^3$$

$$m_p = \rho_w \times V_{Dv50}\ ,\ \text{kg}$$

Where the value of mass density of water (ρ_w) is 997 kg·m^{-3}. Therefore, the theoretical Charge-to-Mass Ratio (CMR) can be calculated as,

$$CMR_{Theoretical} = \frac{q_p}{m_p},\ \text{mC·kg}^{-1} \qquad \text{Equation 8}$$

Understanding the relationship between droplet size distribution, Rayleigh limit, and electrostatic charging efficiency is crucial for optimizing spray systems and electrostatic processes. The Rayleigh limit, also known as the Rayleigh instability

criterion, describes the limiting value of net surface charge, q on an isolated droplet of radius 'r' which may become unstable and lead to the spontaneous formation of droplets when exposed to an external electric field. This instability arises due to the balance between surface tension forces and inertial forces. The value of maximum surface charge or the Rayleigh limit is given as,

$$q_{max} = 8\pi\sqrt{\gamma\varepsilon_0 r^3} \qquad \text{Equation 9}$$

Where, γ is the surface tension of liquid (γ_{water} = 71.78 × 10^{-3} at 25°C) and ε_0 is the permittivity of air (8.85 × 10^{-12} $C^2 \cdot N^{-1} \cdot m^{-2}$). Droplets formed near the Rayleigh limit tend to be small and have a narrow size distribution. These droplets are typically on the order of micrometers or smaller. The size of the droplets influences their charge-to-mass ratio, as smaller droplets have a higher surface area-to-volume ratio and are more susceptible to electrostatic charging. This makes the droplets more responsive to the electric field and more likely to undergo effective charge transfer under electrostatic induction charging. The percentage of maximum droplet charge, or CMR, attained is the measure of an electrostatic induction spray charging system's performance, or charging efficiency (Law,1978 cited by Khatawkar *et al*., 2021).

$$Charging\ Efficiency, \% = \frac{CMR_{achieved}}{CMR_{\text{Rayleigh limit}}} \times 100 \qquad \text{Equation 10}$$

3.4 DEVELOPMENT OF ELECTROSTATIC SPRAYER FOR COCONUT PALMS

The development of an air-assisted sprayer with an electrostatic charging system for coconut palms involves several key subsystems to ensure the proper functioning of the entire unit. The primary focus is on integrating an effective electrostatic sprayer, which requires a high-voltage DC power supply unit as its core component. This is followed by the air assistance system, which provides the necessary airflow to carry the spray droplets to the target area, and the nozzle and liquid delivery system, which

ensures precise and consistent application of the pesticide. The concepts, criteria, and procedures followed for the development of each subsystem are detailed as follows.

3.4.1 Development of high voltage DC power supply

Development of a reliable and efficient high voltage generation (HVDC) system is the critical step involved in the design and development of an electrostatic spraying system. A basic high voltage system is designed to generate and manage high voltages for different applications, as of here is the electrostatic sprayer. Creating a high voltage DC (HVDC) generation system involves several key components, each playing a crucial role in ensuring efficient and safe operation. The basic HVDC system consists of a power source, step-up transformer, rectifier, voltage regulators, heat sinks, high voltage transmission lines, and components for filtering and smoothing the input and output signals

The power source supplies initial electrical energy (DC current from battery or AC from a grid/generator). This supplied voltage is increased to a desired level by step-up transformer. A Line Output Transformer (LOPT) or flyback transformer, operates based on the principles of electromagnetic induction was chosen for the research. The LOPT transformer is an integrated transformer which has built in rectifiers and divider networks and several isolated windings to output different voltages. The primary winding of the LOPT transformer is connected through the DC power source through an oscillator, which is a Metal-Oxide-Semiconductor Field-Effect Transistor (MOSFET) as shown in the circuit diagram (Figure 3). The oscillator circuit generates a high-frequency square signal. This signal is given to the gate of the MOSFET. The MOSFET is turned on and off rapidly by the high-frequency signal from the oscillator. When the MOSFET is ON, it allows current to flow through the primary winding of the transformer, creating a magnetic field in the core. When the MOSFET is OFF, the current flow stops, and the magnetic field collapses. The rapid switching of the MOSFET creates alternating magnetic fields in the transformer core. These alternating fields induce a high voltage in the secondary winding due to the turn's ratio between

the primary and secondary windings. The high voltage output from the secondary winding is then connected to the load.

The voltage regulator, Pulse Width Modulator (PWM) controls the voltage and helps to obtain variable voltage outputs. To ensure a stable DC output, a filter and smoothing circuit comprising of capacitors is used. Heat sinks are also necessary to ensure reliable application as the transformer and MOSFET can generate significant heat. To ensure safety and to prevent electric shock, the circuit is made with high quality electric wires with proper insulation.

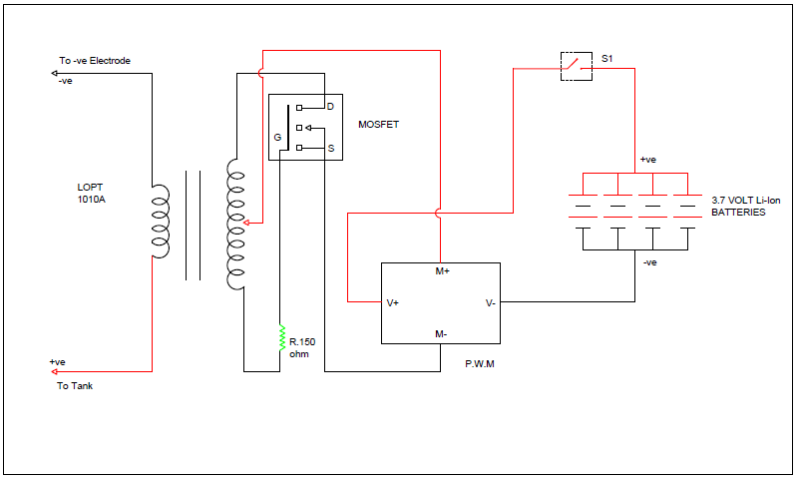

Figure 3. Circuit diagram of HVDC system

3.4.1.1 Development of high voltage electrode assembly

The study employed three embedded ring electrodes made of 4.3 mm thick copper wire of diameters 40, 60, and 90 mm. The electrode with 90 mm diameter was positioned on the outer side of the nozzle-air blower conduit assembly (spray gun) with appropriate insulation. This configuration also allows the electrode to be repositioned to the left or right, enabling the horizontal positioning of the electrode relative to the droplet formation zone to be adjusted as needed. The other two electrodes were housed inside an external groove made on cast nylon sleeves. The constructional details of the electrode carrier sleeves for the 40 mm diameter and 60 mm diameter electrode was given in Figure 4 and Figure 5 respectively. The diverging gradient was provided at the

inner side of the sleeves toward the exit end increases the air velocity, which ensures that the electrode carrier assembly would not hold spray droplets because of electrostatic attraction, thus preventing any possible short circuits between the nozzle and the charging electrode.

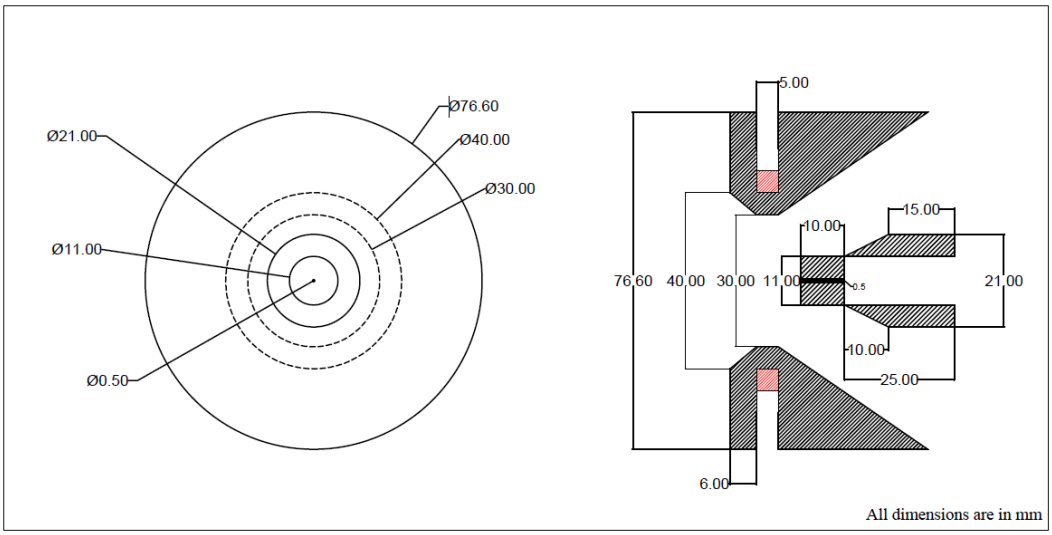

Figure 4. Constructional details of 40 mm diameter electrode carrier sleeve

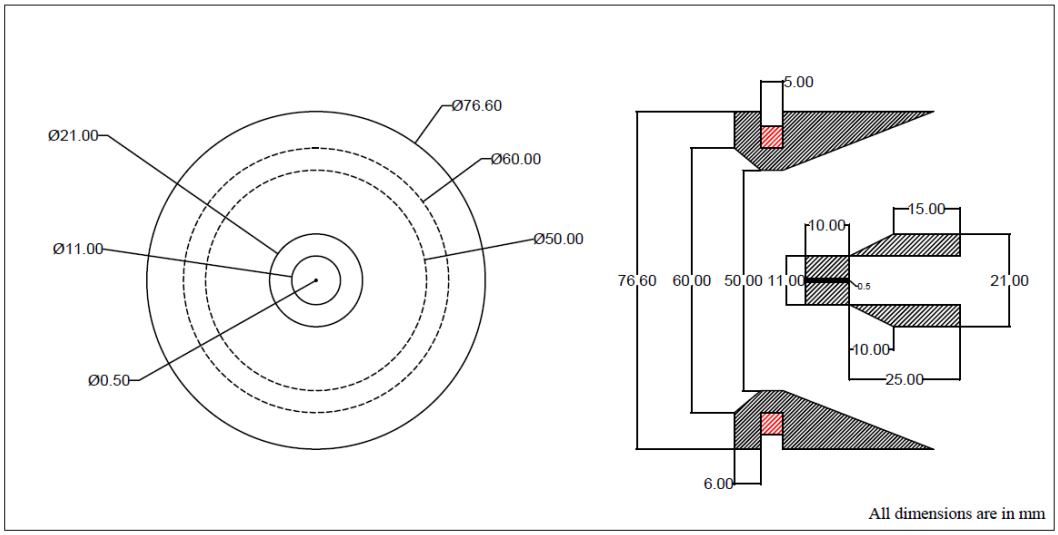

Figure 5. Constructional details of 60 mm diameter electrode carrier sleeve

3.4.2 Development of spray nozzle

The design and development of spray nozzle for sucking pests or flying targets necessitate meticulous consideration of several factors, including spray pattern, droplet

size, coverage, operating pressure and flow rate, and area to be covered. For flying pests, the efficacy of spraying largely depends on the amount of active material reaching the target area and high uniformity of deposition. However, high spray volume can result in pesticide dripping from the foliage. The quantity of pesticides reaching a specific area is directly proportional to spray coverage and inversely related to the droplet size. Therefore, it is crucial to maximize spray coverage to ensure that all surfaces where pests reside are effectively treated (Gan-Mor and Matthews, 2003). The average length of a coconut palm leaf was observed as 3.54 m including the petiole and leaf bearing portion. The spray droplet distribution should be wide enough to cover the entire leaf-bearing portion of the palm.

The droplet size less than 70 µm was more susceptible to loss through evaporation and droplets size larger than 250 µm may susceptible to dripping as well as too large for the application of moving targets. Mist or fog-type sprays with droplet sizes less than 150 µm are suggested for the spraying of flying insects (Zhu *et al*., 1994; George *et al*., 2011; S. Kumar *et al*., 2020). Smith *et al*. (2000) found that the maximum deposition efficiency of pesticides occurred at a droplet diameter of 140 µm and a decline in deposition efficiency was observed with increasing droplet size. The spray nozzle should be able to cover the entire width of coconut palm leaf in a single pass. Considering these droplet spectrum requirements, a hydraulic fogger-type nozzle was selected for the study. The proposed design of the nozzle with the nozzle holder is shown in the Figure 6. The design incorporates a hydraulic fogger-type nozzle threaded at the rear end, securely mounted within a nozzle holder. The nozzle holder features internal threading at the front, matching the nozzle threads to ensure a firm connection, preventing dislodgement under high flow pressures. This assembly is precisely positioned inside the spray gun as shown in Figure 7, ensuring stability and optimal performance.

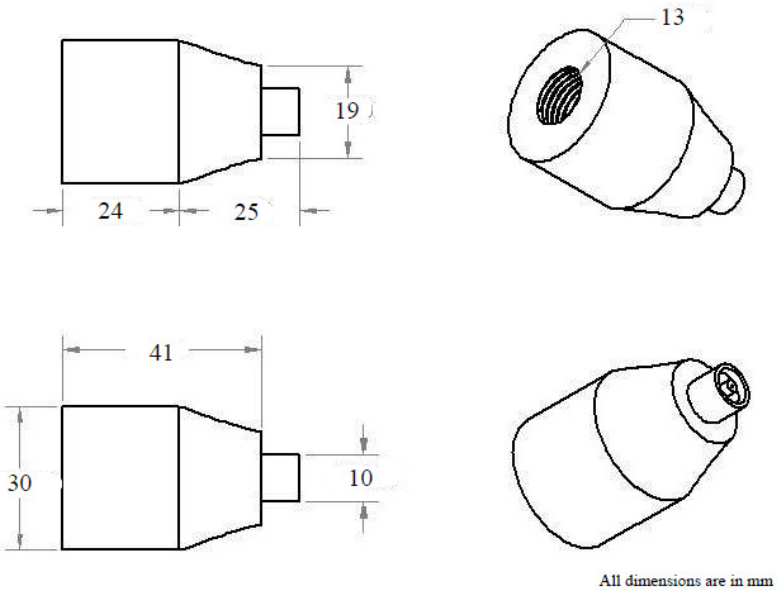

(a)

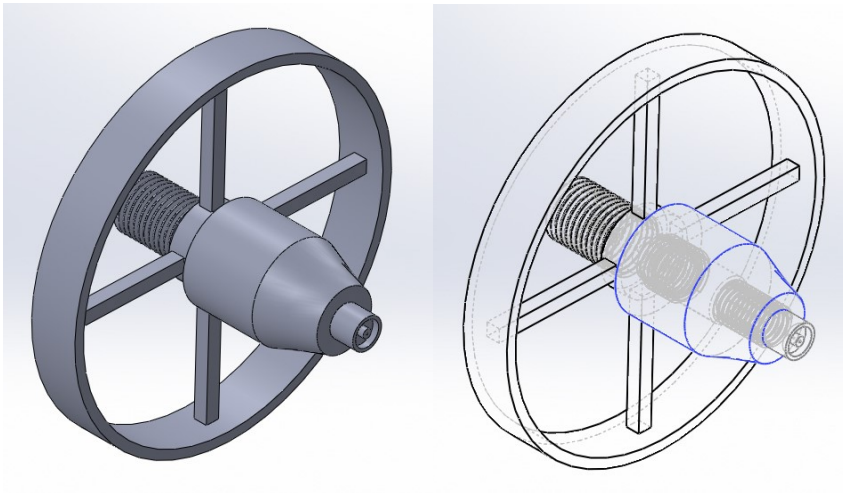

(b)

Figure 6. Arrangement of threaded nozzle and nozzle holder (a) constructional details of nozzle holder (b) nozzle holder with the centring arrangement

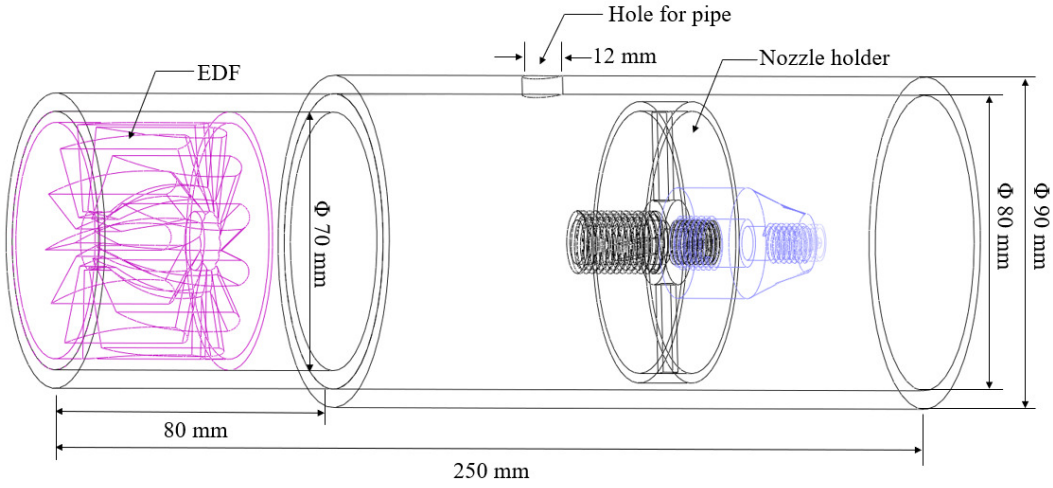

Figure 7. Constructional details of spray gun

3.4.3 Development of liquid delivery system

The selection of liquid delivery system was based on the power source, operational pressure and flow rate requirement of the hydraulic spray nozzle. The power source for the system was a 12 V DC, 9 Ah battery. The pump assembly could be able to deliver liquid formulation at low pressure and low discharge from the tank kept at the back pack of the operator to the nozzle mounted at the top end of adjustable extension pole (15 m approximate length). The operating pressure and flow rate of the spray nozzle was assumed as 6 $kg \cdot cm^{-2}$ and 6 to 7 $L \cdot h^{-1}$ respectively (Patel *et al.*, 2017; Khatawkar, 2019).

The Total Dynamic Head (TDH) is one of crucial factor in selecting the pump for any application. TDH is the equivalent head that a fluid has to be pumped, after considering all the factors that contribute to the resistance against fluid flow. TDH is composed of static head (H_s), Pressure head (H_p), Frictional head loss (H_f) and Minor loss due to pipe fittings (H_{minor}).

$$TDH = H_s + H_p + H_f + H_{minor} \qquad \text{Equation 11}$$

As the pump and the liquid fertilizer tank was at the same level, static head (H_s) can be ignored. The value of pressure head, 60 m was determined from the water column corresponding to nozzle operating pressure (6 kg·cm^{-2}). Friction head loss (H_f) is calculated using the Darcy-Weisbach equation as follows.

$$H_f = \frac{fLv^2}{2gD} \qquad \text{Equation 12}$$

Where '*f*' is the Darcy's friction factor, '*L*' is the total pipe length (m), '*v*' is the flow velocity (m·s^{-1}), '*D*' is the hydraulic diameter of pipe (m), and '*g*' is the acceleration due to gravity (m·s^{-2}).

The pipe or hose for carrying the pesticide-water solution was 10 m long (*L*) polyurethane hose with an external diameter (OD) of 10 mm and internal diameter (ID) of 6.5 mm. The flow velocity, v through the pipe was determined from discharge 7 L·h^{-1} and ID 6.5 mm was 0.058 m·s^{-1}. Reynolds number for the flow through the pipe, R_e was determined using the following equation,

$$R_e = \frac{vD}{V} \qquad \text{Equation 13}$$

(*V* is kinematic viscosity of water and its value is 1 mm^2·s^{-1} at 20ºC)

Substituting the corresponding values in Equation *13*, R_e was obtained as 377. Since, R_e<2000, the flow is laminar. Darcy's friction factor, '*f*' for laminar flow is given as Equation 14 (Bai and Bai, 2019).

$$f = \frac{64}{R_e} \qquad \text{Equation 14}$$

$$f = 0.1697$$

Hence, using Equation 12, H_f = 0.06714 meters

Minor loss due to pipe fittings and bents, 'H_{minor}' was determined using the following equation:

$$H_{minor} = \frac{Kv^2}{2g} \qquad \text{Equation 15}$$

Where '*K*' is the loss coefficient for pipe fittings, The value of *K* for regular threaded 90º elbow joint (1 Nos), ball valve (1 Nos), and unions /connectors (3 Nos) were 1.5, 5.5, and 0.24 (3×0.08) respectively. Hence, the value of H_{minor} was calculated as 0.012 m. considering all the heads into the Equation 11, the TDH was calculated as,

$$TDH = 0 + 60 + 0.06714 + 0.0012 = 70.06\ meters$$

Hence, from TDH the pressure required to develop by the pump was calculated as 7 kg·cm^{-2}. Therefore, a 12 V battery operated double stage diaphragm pump of 10 L·m^{-1} discharge with 10 kg·cm^{-2} cutoff pressure was selected for the study as shown in Figure 8.

Figure 8. Double stage diaphragm pump

3.4.4 Design of battery – operated air – assistance unit

The selection of suitable air-assisting methods plays a pivotal role in optimizing the efficiency, efficacy, and environmental sustainability of air-assisted spraying in agriculture. The choice of air-assisting method profoundly influences spray quality, defined by droplet size distribution, velocity, and trajectory. Finer spray droplets accompanied by the air-assisting techniques can results in deeper penetration into the dense crop canopies, uniform deposition, less spray volume, and reduced drift (Delele *et al*., 2005). The choice of an air assisted unit for agriculture operation must be based on factors including the type of crop canopy, target pest, prevailing weather conditions, and equipment specifications. Considering the design requirements of the research, specifically the spraying of coconut palms using an electrostatic nozzle mounted on top of an 8 m long telescopic pole, it is of vital importance that the weight of the blower assembly remains within limits to avoid balancing issues and operator fatigue. Nonetheless, the assembly must generate sufficient thrust force to propel the spray droplets against gravity, ensuring penetration into the canopy and effective targeting of the desired areas.

3.4.4.1 Theoretical analysis of air volume and air flow

The calculation of theoretical demand of air flow volume and air flow velocity of the air-blower system was based on the 'displacement principle of air volume' and 'terminal velocity principle of air flow' respectively (Jin *et al*., 2018; Miao *et al*., 2023; Wei *et al*., 2023). The air assistance unit should be capable of transporting the air flow from the fan outlet to the palm canopy and also penetrate through the canopy. According to the principle of displacement of air volume, the displacement area should be the area between the sprayer outlet and boundary of the canopy as shown in the Figure 9. The volume of air generated by the fan per second due to the movement of sprayer and the constant rotation of fan is equal to the area of the rectangle (shaded portion). Hence, equation for the required air volume or fan delivery ($Q_{required}$ in $m^3 \cdot s^{-1}$) is given as:

$$Q_{required} = v(d + L)(H_1 + H_2)K_1 \qquad \text{Equation 16}$$

Where 'd' is the width of spray gun (m), 'v' is the operating speed of sprayer (m·s^{-1}), 'H_1' is the height from the tip of spray gun to the bottom leaf of palm (m). 'H_2' is the height of canopy, and 'K_1' is the coefficient of airflow attenuation and losses along the way (1.3−1.6).

According to the terminal velocity principle of air flow, the velocity of air flow must have a minimum level as when it reaches the end of its target range. This ensures the penetration and adhesion of droplets within the crop canopy. The equation for the terminal velocity is as follows:

$$V_2 = K_2 \frac{V_1 d}{L} \qquad \text{Equation 17}$$

From the above equation, the velocity required at the discharge outlet is yield as:

$$V_1 = \frac{V_2 L}{K_2 d} \qquad \text{Equation 18}$$

Where, 'V_1' is the initial velocity at the outlet in m·s^{-1}, 'V_2' is the end velocity in m·s^{-1}. 'L' is the spraying swath in m, and 'K_2' is the coefficient of air resistance and frictional loss along the flow path (1.3 to 1.8).

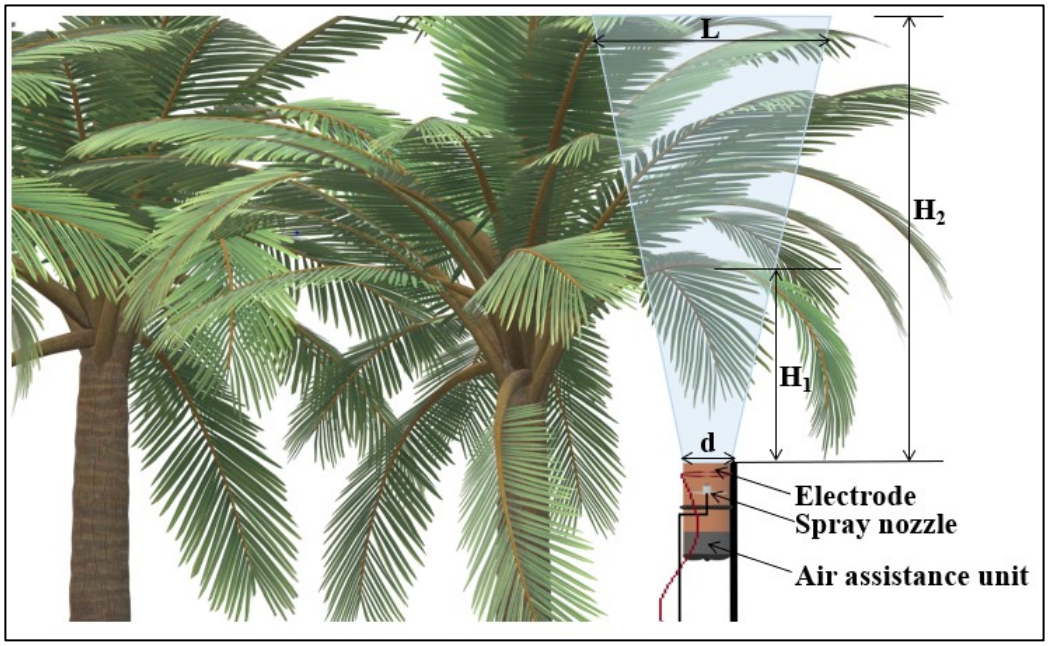

Figure 9. Air displacement diagram of the electrostatic sprayer for coconut palms

3.4.4.2 Selection of air-assistance unit or Electric Ducted Fan (EDF)

Given the outlined considerations, the most appropriate choice for air assistance is to utilize an Electric Ducted Fan (EDF) as the air assistance unit. Because of their high thrust-to-weight ratio and thrust-to-fan diameter ratio, quietness and compactness. In addition, they are easier to construct and operate (Jin *et al.*, 2018; Urban *et al*., 2023).

Electric Ducted Fan (EDF) is basically a small fan or propeller set in an enclosed tube or duct, which is powered by an electric motor. The rotation of the fan/impeller sucks air from one side and pushes it out at the back side at a high-speed creating a thrust. The EDF has three major components: the inlet/entry duct, the compressor/fan, and the nozzle/exit duct. The dimensions of these major parts have major influence on the performance of the EDF. The design of an EDF is based on the thrust force required in the system. Thrust is the force required to overcome gravity and move an object or provide the desired acceleration, it is generated through the reaction of accelerating a mass of air. (Benson, n.d.; van Oorschot, 2018; Zhang and Barakos, 2020).

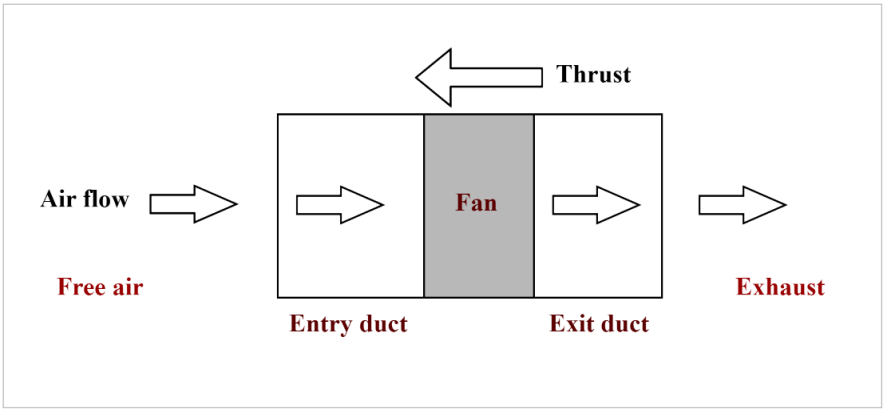

Figure 10. Schematic diagram of an Electric Ducted Fan (EDF)

The thrust developed by an EDF was calculated using the general thrust equation (van Rooij, 2019),

$$Thrust\ (T)\ =\ T_p + T_d \qquad \text{Equation 19}$$

Where T_p is the thrust force directly generated by the fan blades and T_d is the thrust force developed due to the pressure force inside the duct. The thrust force due to the pressure difference, T_d was calculated as,

$$T_d\ =\ \Delta p \times A$$

$$T_d\ =\ \frac{1}{2}\rho\ ({V_2}^2 - {V_1}^2) \times A \qquad \text{Equation 20}$$

From Newton's second law of motion, the force (F) is defined as the change in momentum of an object with a change in time (t). Whereas, momentum is the object's mass (m) times the velocity (V). Accordingly, the equation for the force can be written as:

$$Force\ (F)\ = \frac{(mV_2) - (mV_1)}{(t_2 - t_1)}$$ Equation 21

Since the mass is constant and change in velocity with time is the acceleration, 'a' the above equation can be simplified as:

$$Force\ (F)\ = ma$$

Figure 10 shows the schematic representation of an EDF with inlet and exit duct with area of A_i and A_e respectively, and a fan of diameter D_f. As the fan blades rotates, they draw air into the unit through the inlet duct with a velocity V_i. The spinning action of the blade accelerated and compresses the air. This accelerated air then expelled out through the exit duct with a high velocity V_e. based on the Newton's third law of motion, the expelled air creates a reactionary force, called thrust (Urban *et al*., 2023). As per the law of conservation of mass,

$$Q_i = Q_e$$ Equation 22

$$A_iV_i = A_eV_e$$ Equation 23

Where Q_i and Q_e is the volume of air passing in unit time through inlet and exit ducts. The mass of air being moved or the mass flow rate, M in kg·s^{-1} can be determined as (Junaidin and Cahyono, 2019):

$$M\ = \rho Q_i$$ Equation 24

Where ρ is the density of air (1.224 kg·m^{-3} at Standard Sea Level). The increase in air speed generated by the ducted fan is determined by the difference between the inlet air velocity and the exit air velocity through the duct.

$$dV = V_e - V_i \qquad \text{Equation 25}$$

The thrust, 'T_p' produced as a result is calculated by considering the increase in momentum of moving air mass, which is the product of mass flow rate and the increase in velocity. Hence, the Equation 20 can be re-written as:

$$T_d = M\,dV \qquad \text{Equation 26}$$

Hence, the general equation becomes,

$$Thrust\ (T) = M\,dV + \frac{1}{2}\rho\,({V_e}^2 - {V_i}^2) \times A$$

3.4.4.3 Power required for the EDF

The power acquired by the system due to the inflow of air mass is termed as P_{gain}, which is given by the kinetic energy of the moving air mass entering the system.

$$P_{gain} = \frac{1}{2}M{V_i}^2 \qquad \text{Equation 27}$$

Similarly, the power lost from the system, P_{loss} as a result of expelling out air mass is given as:

$$P_{loss} = \frac{1}{2}M{V_e}^2$$

The power developed by the fan, P_{fan} can be determined by considering the conservation principle as,

$$P_{fan} = P_{loss} - P_{gain}$$

The power required for the motor to operate fan, $P_{motor,}$ after considering the efficiency of the motor (generally taken as ~ 85%) and losses in the system due to geometry restrictions and friction in the duct (Ajraoui, 2019; Junaidin and Cahyono, 2019) was calculated as:

$$P_{motor} = \frac{P_{fan}}{0.85} \qquad \text{Equation 28}$$

3.4.4.4 Conditions for static operation

An electric ducted fan (EDF) is primarily employed for aircraft propulsion, particularly for model aircraft and small unmanned aerial vehicles (UAVs). However, under static conditions (zero forward velocity), the EDF functions similarly to its operation in flight. Since, this research is utilizing the EDF in a stationary position to provide airflow for an air-assisted electrostatic sprayer, it is crucial to understand the performance under static conditions.

Under static operating condition, the forward velocity is zero and the assumption of same inlet and exhaust velocity becomes invalid, as there is a significant difference between the inlet and exit velocities (van Oorschot, 2018; Urban *et al.*, 2023). As the air is sucked into the system from a region of still air, the velocity of inlet air, V_i is infinitesimal. Hence, it was assumed that the change in velocity (dV) closely approximates the exit velocity (V_e) and the power gained system by means of kinetic energy of inlet air was approaching zero i.e. $P_{gain} = 0$ (Sharman, 2011).

$$P_{fan} = P_{loss} - P_{gain} = P_{loss} - 0$$

$$P_{fan} = P_{loss} = \frac{1}{2} M V_e^{\,2} \qquad \text{Equation 29}$$

The equation for thrust becomes,

$$T\ (static)\ =\ M\ V_e + \frac{1}{2}\rho {V_e}^2 A \qquad \text{Equation 30}$$

3.4.4.5 Fabrication of Electric Ducted Fan

The most important design parameter of an EDF is the clearance between the blade tip and inner wall. The other major factors influencing the design are diameter of fan and leading edge, no. of blades, power and kV rating of electric motor. These factors directly influence the structure as well as the performance of the EDF. A prototype of EDF was drawn using the SOLIDWORKS 3D CAD modelling software (SolidWorks Corp., Waltham, MA, USA). Each part of the EDF including blade, outer shell or duct, and nozzle were drawn as separate part in the software and subsequently fabricated using 3D printing technology. The 3D printer (UltiMaker) works on Fused Deposition Modelling (FDM) technology, which fabricate a model by folding the printing material into individual layers. The printing material was Polylactic acid (PLA), which require a comparatively low printing time. The Figure 11 shows the 3D drawing and the printed prototype of the EDF.

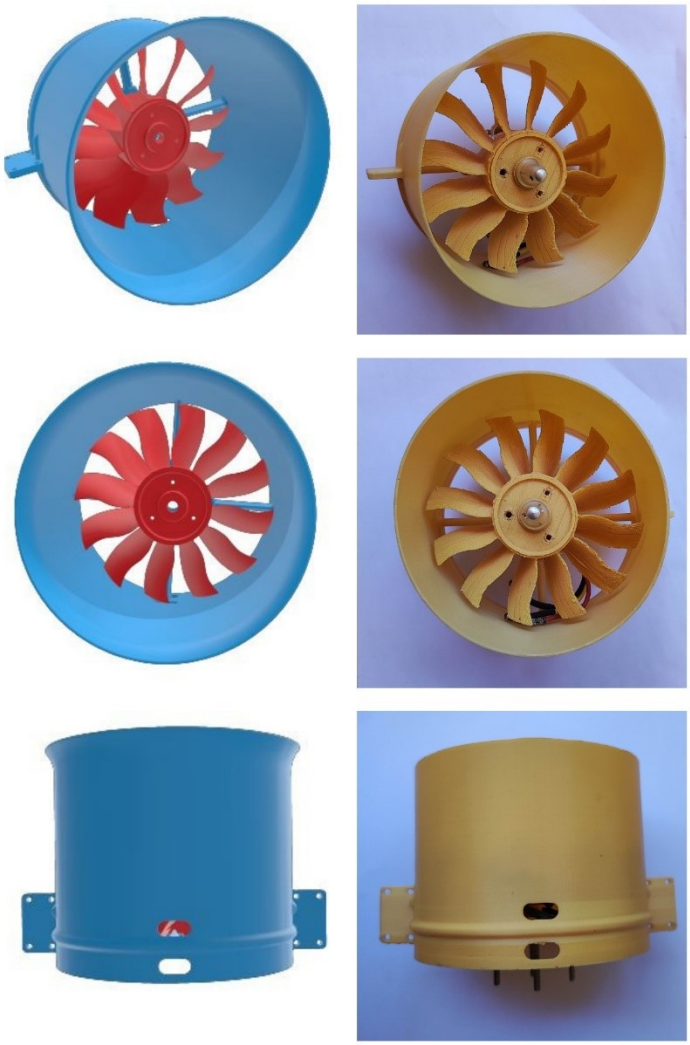

Figure 11. Three-dimensional drawing and 3D printed model of EDF

The fabricated prototype was operated with 1800 kV brushless motor (model: A2212) and powered by a 12 V DC battery (same used for driving the pump). The observed maximum airflow velocity of the Electro-Driven Fan (EDF) was recorded at 12.17 $m \cdot s^{-1}$, which failed to meet the minimum flow velocity requirement. Additionally, when operating the sprayer equipped with the 3D-printed fan, it was noted that the airflow was dispersing laterally rather than maintaining a concentrated, linear trajectory. This dispersion led to a broader and more erratic distribution of spray droplets. These issues are likely attributable to the high surface roughness inherent to the Fused Deposition Modelling (FDM) printing process, coupled with low production tolerance

and more clearance between the inner casing walls and the blade tips. The limitations of 3D printing, including its impact on precise fitting and finishing, adversely affect the performance of the prototype. Hence, a commercially available ducted fan with the same diameter and number of blades were purchased. The details of the commercially available EDF were given in the Table 1.

Table 1. Details of 3D printed and Commercially available EDF

Item	3D printed EDF	Commercially available EDF	Design requirements
Fan diameter, mm	70	70	90 mm (Max)
Volt, V	12	12	Suitable
Ampere, A	45	45	Suitable
Watts, W	540	540	169.11 (Min)
Thrust at full throttle, kg_f	1.16	2.24	1.62
Motor model	QF2827	QF2827	Suitable
Motor kV rating	1800 kV	1800 kV	Suitable
Electronic Speed Controller (ESC), A	80	80	Suitable

3.4.5 Adjustable spray extension pole

To address the drawbacks of conventional sprayers, such as spraying in large quantities. It was determined that spraying should be done near the coconut palm canopy. Specifically, the spray nozzle should be positioned to reach approximately 1 to 2 m below the lowest palm leaf. To achieve this, the design involved mounting the spray nozzle, along with an air-assistance unit and a high-potential electrode, on a long pole. The selection of the pole's type and material was critical; it needed to be strong enough to support the nozzle-air blower assembly while remaining lightweight to facilitate easy handling and transport by a single operator. This aims to enhance

spraying efficiency, reduce pesticide waste, and minimize environmental impact by ensuring precise application directly to the target area.

3.4.6 Backpack frame

A backpack frame was designed to accommodate the primary weight-bearing components, including the spray solution tank, battery, and pump. The dimensions of the backpack frame were determined based on the space requirements of these components. Material selection for the fabrication of the backpack frame prioritized overall weight, reliability, and corrosion resistance.

The backpack frame was constructed using 25 mm PVC pipes, chosen for their lightweight yet sturdy properties, which provide a strong and reliable structure without adding unnecessary weight. The use of PVC pipes ensures that the frame remains durable and resistant to environmental factors, such as moisture and corrosion, which are common in field conditions.

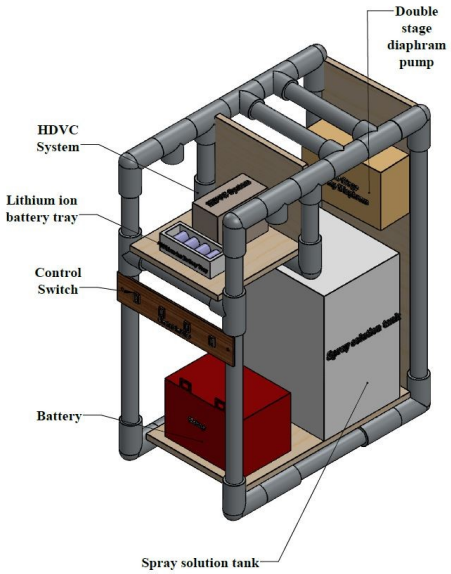

Figure 12. Schematic diagram of backpack frame

To further enhance the practicality and weight distribution of the frame, the compartments and the base were made from 3 mm thick plywood sheets. Plywood was selected due to its excellent strength-to-weight ratio, ensuring that the frame can

support the load of the components while keeping the overall weight manageable. The 3 mm thickness of the plywood provides adequate support and stability for the housed components, preventing deformation and ensuring longevity. The proposed design of the backpack frame is given in Figure 12.

3.5 LABORATORY EXPERIMENTS

Before conducting field evaluations of the developed air-assisted electrostatic sprayer for coconut palms, it is essential to optimize its key operational parameters through laboratory studies. These parameters include the Charge-to-Mass Ratio, electrode voltage, electrode diameter and positioning relative to the nozzle, and the droplet spectrum generated by the electrode. The detailed procedures followed for these laboratory experiments are discussed below.

3.5.1 Development of laboratory experimental Set-up

To measure the Charge-to-Mass Ratio, a specially designed Faraday cage was employed. The Faraday cage comprises two inverted conical structures made of a 4.3 mm thick copper wire frame and a copper wire mesh with a 1 mm aperture. The bottom section of the cage was fabricated in a truncated conical shape, while the top section was fully conical, both with a base diameter of 500 mm and a cone angle of 45°. This structure was suspended on a cantilever beam at the top end of a 4.0 m long telescopic pole. A sliding cantilever beam was positioned below to hold the spray gun, ensuring that it place exactly below at the center point of the cage as illustrated in Plate 2. This design allows for adjustable spacing between the cage and the spray gun, ensuring effective capture of all droplets by the cage. The Faraday cage was connected to the earth potential through a digital multimeter (KUSAM-MECO Brymen, Ind. Ltd., Model No. KM-5040T/BM-812a). The experiment was conducted under controlled indoor conditions to eliminate the influence of weather parameters, such as wind, which could potentially affect the accuracy of the measurements.

3.5.2 Measurement of charge-to-mass ratio (CMR)

The amount of charge imparted on the spray jet is directly proportional to the magnitude of electric potential. The charge-to-mass ratio implies the chargeability of the spray droplets by the electrode held at high electric potential.

The high voltage potential in the range of kilovolts (4 to 10 kV) of the electrodes were measured using a high voltage probe (KUSAM-MECO Brymen, Ind. Ltd., Model No. PD-28) as shown in the Plate 1. The spray cloud current was measured at different combinations of electrode potentials, electrode diameter, and horizontal position of electrode relative to the nozzle. The electrode potentials was varied between 4 to 10 kV with 1 kV measuring interval (Mamidi *et al*., 2013; Martin and Latheef, 2017). The internal diameter of electrode was chosen as 40, 60 and 90 mm (Patel *et al*., 2013; Khatawkar, 2019), and horizontal position of electrode relative to the nozzle was varied between 5, 10, and 15 mm towards the front (Maynagh *et al.*, 2009; Patel *et al*., 2013). The radial distance was changed by using electrodes of different radii and the horizontal position was varied by displacing the cast nylon electrode carrier sleeve towards the front side. All observations were recorded at vertical distances of 1 m and 2 m between the Faraday cage and the spray gun. The flow rate of the nozzle was 79.8 $mL \cdot min^{-1}$ and the current was measured for 60 seconds with the EDF operated at an air velocity of 17 $m \cdot s^{-1}$. The charge-to-mass ratio, expressed in $mC \cdot kg^{-1}$ was calculated as the ratio of spray cloud charge (μA) to the mass flow rate of spray liquid ($kg \cdot s^{-1}$). The charging efficiency of the developed electrostatic system was then determined based on electrode potential at which the maximum charge-to-mass ratio observed. The charge carrying capacity of the optimized electrode-voltage composition was determined by varying the relative position (vertical) between Faraday cage and the spray gun. The measurements were done at 1,1.5, 2 and 2.5 m distance between the spray gun and Faraday cage.

High Voltage Probe

Digital Multimeter

Plate 1. Instruments for measurement of high voltage

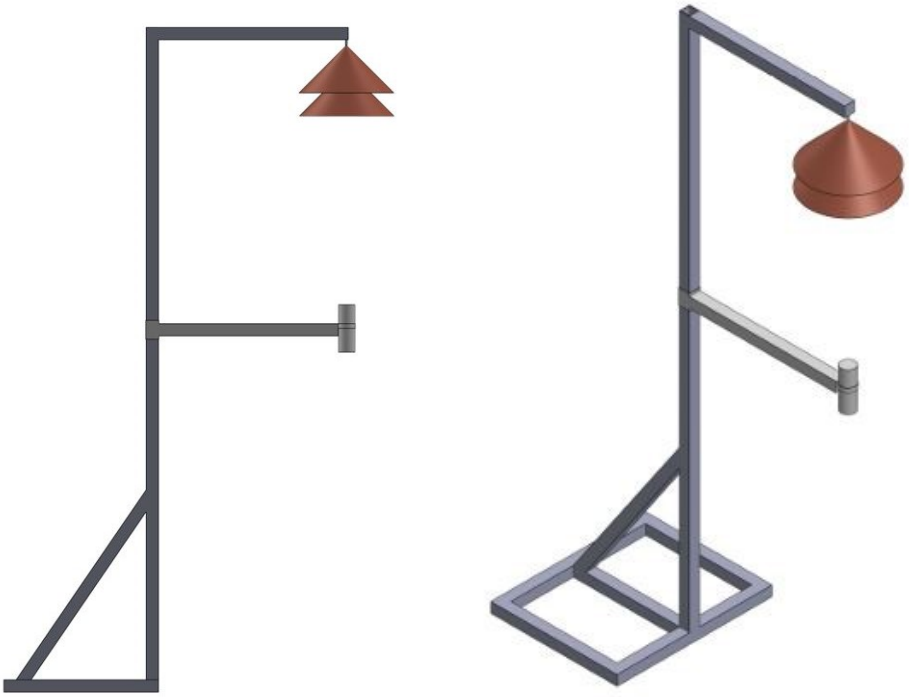

Figure 13. CAD of Faraday Cage experimental setup for CMR measurement

Plate 2. Faraday Cage experimental setup for CMR measurement

3.5.3 Determination of droplet spectrum

The spray droplet spectrum is a critical factor in agricultural spraying as it provides detailed information about the size distribution of the droplets, which in turn influence the spray coverage, efficacy, optimum penetration, drift reduction and overall efficiency. The droplet spectrum was determined using Water-Sensitive Paper (WSP) measuring 26 × 76 mm (Aadhaar Green Solutions, Delhi). To optimise the operating pressure for generating a finer droplet spectrum, the sprayer was tested at three different pressures including 3, 4, and 5 kg·cm^{-2} (Khatawkar *et al*., 2021; Dai *et al.*, 2022). The EDF was operated at the lower speed to avoid the droplet spread caused by the high velocity impact. The observations were made under both electrostatic charging ON and OFF conditions to evaluate the impact of electrostatic charging on droplet atomisation. After spraying the WSPs are allowed to dry and then transferred into zip lock cover and later scanned at 600 dpi resolution using Epson M2170 scanner. The scanned images were analysed using 'DepositScan' software, a publicly available ImageJ software developed by USDA-ARS Application Technology Research Center for

droplet spectrum in terms of droplet size distribution (DV_{10}, DV_{50}, and DV_{90}), droplets per unit area, and percentage coverage.

The actual diameter of the droplet from the spot area in the 'DepositScan' software was calculated using the following equation (Zhu *et al*., 2011):

$$d = 0.95 d_s^{0.910} \qquad \text{Equation 31}$$

Where d_s can be calculated from,

$$d_s = \sqrt{\frac{4A}{\pi}} \qquad \text{Equation 32}$$

Where, A is the spot area in μm^2. The final actual droplet diameter, D was calculated from the following equation,

$$D = 1.06 A^{0.455} \qquad \text{Equation 33}$$

3.5.3.1 Volume Median Diameter (VMD)

The most widely used parameter to assess droplet size is the volumetric diameter DV_{50} measured in μm, also referred to as the "Volume Median diameter" (VMD or DV_{50}), which divides the spray into two equal parts based on the sprayed volume, with 50% of the total volume contained in droplets smaller than the VMD and the remaining 50% in droplets larger than the VMD. The volume median diameter is utilized to characterize the spray quality of a nozzle by indicating the average droplet size relative to the total volume sprayed. The VMD provides insight into drift risk, like very fine droplets may be carried by the air around stems and leaves. Fine to medium droplets are ideal for depositing on stems and narrow vertical leaves, and coarse droplets are best for large, flat surfaces like broadleaf weeds or soil applications (Matthews, 1989; Privitera *et al*., 2023).

3.5.3.2 Number Median Diameter (NMD)

The diameter that refers to the number of droplets is known as the Number Median Diameter (NMD) or volumetric diameter DN_{50}), which represents the point where 50% of the total number of droplets are smaller than this diameter. Generally, the NMD is smaller than the VMD. The NMD emphasizes the contribution of all droplets, including the smallest ones. VMD is more influenced by a relatively small number of large droplets, while the NMD is more affected by the smaller droplets. Therefore, the more uniform the droplet sizes are, the closer the ratio of VMD to NMD approaches unity (Matthews, 1989; Privitera *et al*., 2023).

3.5.3.3 Uniformity coefficient (Uc)

Uniformity coefficient is a factor indicating the uniformity of the droplet spectrum measured as the ratio of VMD to NMD. VMD is more influenced by a relatively small number of large droplets, while the NMD is more affected by the smaller droplets. Therefore, the more uniform the droplet sizes are, the closer the ratio of VMD to NMD approaches unity (Hanafi *et al*., 2016; Privitera *et al*., 2023).

$$Uc = \frac{VMD}{NMD} \qquad \text{Equation 34}$$

3.5.3.4 Relative Span Factor (RSF)

Relative span factor (RSF) is a dimensionless value indicates the width of the droplet size distribution. It is calculated as the ratio of the difference between DV_{90} and DV_{10} to the value of DV_{50}. A smaller RSF value significances the smaller width of droplet spectrum with less variation in the droplet sizes, which results in more consistent coverage and reduced drift (Privitera *et al*., 2023).

$$RSF = \frac{DV_{90} - DV_{10}}{DV_{50}} \qquad \text{Equation 35}$$

3.6 DEVELOPMENT OF ELECTROSTATIC SPRAYER PROTOTYPE

An electrostatic sprayer prototype was developed based on optimized field parameters identified through laboratory studies, which was then followed by evaluation under actual field conditions. The primary components of the prototype include a spray gun, a telescopic pole, and a backpack frame. The spray gun (mounted vertically at the top of a telescopic pole with the maximum reach of 8 m) incorporates the nozzle, an air-assistance unit (EDF), and a high-voltage electrode to enhance spray delivery. Whereas, the backpack frame houses essential elements, including a 12V DC battery, HVDC system, pump assembly, and all control interfaces, enabling efficient operation and ease of use in field applications.

During operation, the operator first activates the EDF unit, setting it to the desired speed via the Electronic Speed Controller (ESC) to generate an optimal air-assisted spray. Once the EDF is set, the pump and HVDC systems are switched on simultaneously. The flow rate of the pump is adjusted using a bypass flow control lever, allowing precise control of the spray output, with pressure monitored through a pressure gauge 5 $kg \cdot cm^{-2}$. At this stage, the nozzle initiates the ejection of the spray spectrum, while the HVDC system's voltage regulator is set to generate the required high voltage (9 kV). The positive terminal of the HVDC setup was given the spray solution tank as a ground and its negative terminal to a high-voltage electrode, measuring 43 mm in diameter and positioned 10 mm in front of the nozzle.

As droplets are ejected and pass near the high-voltage electrode, a positive charge is induced on the electrode, promoting secondary atomization that further reduces droplet size for improved coverage. The positively charged spray droplets are directed toward the negatively charged plant canopy, enabling an efficient electrostatic attraction. Upon contact with the canopy, each droplet neutralizes at its impact point, which prevents additional droplets from accumulating in the same area. This self-regulating feature optimizes spray distribution across the canopy, reducing over-application and minimizing spray liquid wastage. As a result, the sprayer delivers

precise, uniform coverage while enhancing resource efficiency and reducing environmental impact.

3.7 PERFORMANCE EVALUATION OF THE PROTOTYPE

The performance of the developed prototype of air-assisted electrostatic sprayer was evaluated under actual field conditions in terms of droplet size, percentage coverage, droplet density and spray deposition. The trials were conducted at Instructional Farm of KCAEFT, Tavanur. Considering the challenges of accessing the upper canopy of coconut palms, the trials were conducted on palms with a maximum height of 6 meters and the average length of an individual leaf was 3.5 m. The palm canopy was divided into three sections, Bottom (B), Middle (M) and Top (T) for the measurements. The sprayer was operated at 5 $kg \cdot cm^{-2}$ and discharge of 7 $L \cdot h^{-1}$. During spraying the operator moved around the coconut palm in a uniform speed.

3.7.1 Performance assessment of air -assistance unit

The optimum operation parameters of the air -assistance unit (EDF) including the air velocity at the blower outlet and operating distance were determined at the field trials. The air assistance unit was operated at three different velocities (blower speed) 10, 15, and 17 $m \cdot s^{-1}$ respectively and the EDF was positioned at 1, 1.5 and 2 m below the canopy. The air velocity was measured using a digital anemometer (M/s. ACD Machine Control Company Private Limited, Mumbai).

3.7.2 Performance assessment of the developed electrostatic sprayer

The field evaluation of the developed sprayer was carried out using the optimized operating conditions established during laboratory studies and prior field trials. These conditions included an operating pump pressure of 5 $kg \cdot cm^{-2}$, a blower speed of 17 $m \cdot s^{-1}$ and operation from 1.5 meter below the canopy. The electrostatic system was set to operate at an electrode potential of 9 kV with an electrode of diameter 90 mm. Trials were conducted under both electrostatic charging ON and OFF conditions to assess the impact of electrostatic charging of droplet during spraying. The results were compared with conventional sprayer (Rocker sprayer)

3.7.2.1 Quantification of spray deposition

The spray deposition was calculated using leaf wash method, with the real coconut leaf as natural collectors. A water-based dye, Tartrazine (E-102) used for the spray deposition analysis as it was non-toxic, relatively less costly, high recovery rate and involves simple laboratory procedures (Pergher, 2001). The dye was mixed with the spray liquid in a concentration of 10 $g \cdot L^{-1}$ (Balsari *et al*., 2007; Gil *et al*., 2014). The sprayer was operated initially for 60 and 30 seconds prior to the field trials and observed that dripping from the bottom leaves while spraying for 60 seconds and hence the field trials were conducted with spraying for 30 seconds. The sample solution from the tank was collected prior to the testing to determine the actual tracer concentration. Also, three sample leaf cuts (10 × 50 mm) randomly taken from the palm were collected and placed in plastic bag. For the deposition analysis method, the collected sample leaves were washed with 20 mL distilled water. The washings were later analysed using spectrophotometer.

3.7.2.2 Spray drift

The spray drift measurements of agricultural sprayers play a vital role in environmental protection by assessing the off-target spray deposition. Furthermore, it helps in enhanced precision in application, leading to improved pest management efficacy ensuring that only the target area or crops were exposed to the spray droplets. The off-target spray droplet observations were taken by arranging the WSPs at ground level with equal horizontal spacing aligned in the direction of prevailing wind. The WSPs were positioned at various distances from the canopy, starting from the point of spraying, which was considered as 0 meters, and extending to 1, 2, 3, and 4 meters. To ensure stability against wind, the WSPs were securely fastened with paper clips. The experiment was conducted on a levelled surface to maintain consistency in measurements. The spray drift is measured as the spray deposited per unit area of the WSP (Bueno *et al*., 2017).

3.7.2.3 Sampling procedure

The droplet spectrum and coverage were determined using the water-sensitive papers (WSP) of size 26 × 76 mm (Aadhaar Green Solutions, Delhi). The WSPs were (are fixed with clip) positioned at the abaxial and adaxial side of the top (T), middle (M) and bottom (B) leaves. The sprayer was operated for 30 seconds at a single location and waited some time for the water sensitive papers and the leaves to dry. The WSPs were collected carefully and then transferred to zip lock covers and stored under shade until processed. Each WSPs were then scanned at 600 dpi resolution using Epson M2170 scanner.

3.7.2.4 Data analysis

The droplet spectrum, percentage of spray coverage, droplet density, and spray deposit per unit were determined by analyzing the WSPs using 'DepositScan' software as explained under section 3.8 droplet spectrum analysis. The spray deposition was determined by the leaf wash method. The concentration of tracer in the sample washings from the field trials were calculated by measuring the optical absorbance at wavelength of 427 nm under UV spectrophotometry (double beam spectrophotometer HITACHI U-2900/2910). The spray deposition, d ($mg \cdot cm^{-2}$) was calculated using the equation (Pergher and Gubiani, 1995; Llop *et al*., 2015),

$$d = \frac{T_{cl} \times w}{S_a} \qquad \text{Equation 36}$$

Where 'T_{cl}' is the tracer concentration of the sample in $g \cdot L^{-1}$. T_{cl} is determined from the calibration graph by plotting the absorbance value in the ordinate and their known concentration in abscissa. 'w' is the volume of distilled water used to wash the sample in mL and 'S_a' is the exposed surface area in cm^2. As the tracer concentration may vary for each treatment, a normalized deposit, d_n ($mg \cdot cm^{-2}$ leaf/ $mg \cdot cm^{-2}$ leaf ground) was calculated according to the following equation,

$$d_n = \frac{d \times 10^5}{V \times T_{cs}} \qquad \text{Equation 37}$$

Where 'V' is the application rate per ha (84 L·ha^{-1}) and 'T_{cs}' is the tracer concentration for treatments in mg·L^{-1}, and 10^5 is a conversion factor.

The percentage of spray retained was calculated using the given equation (Llorens *et al*., 2010; Salcedo *et al.,* 2020),

$$\text{D}, \% = \frac{d \times 10^7 \times \text{LAI}}{V \times T_{cs}} \qquad \text{Equation 38}$$

Where LAI, is the Leaf Area Index

3.7.3 Biological efficacy

Biological efficacy of the developed sprayer was evaluated by the effectiveness in controlling the Rugose Spiraling Whiteflies (RSW) in coconut palms. The bio-efficacy of the air-assisted electrostatic sprayer, air-assisted sprayer and conventional hydraulic sprayer (Rocker sprayer), and control (no spraying) was estimated as the pre and post treatment count of RSW population in coconut leaves. The treatments were applied to four replicates with 5 palms per replication. The insecticide Actara (Thiamethoxam a.i. 25% w/w) at a rate of 2.5 g per 10 L was used for all the treatments. The pre-treatment pest count was recorded 24 hours before treatments. and post-treatment pest count was recorded at 1, 4, 7 and 15 days after treatments.

The observation of RSW incidence was recorded as percentage of leaves infested per palm, severity of pest damage and number of pests per leaflet. The percentage of leaf infested per palm was estimated as the number of leaves infested by the pest to the total number of leaves. Severity of damage was assessed by the number of leaflets affected to the total number of leaflets in a leaf. Whereas the pest count was recorded by counting the number of RSW and presence of live egg spirals of each

coconut. The results were analyzed based on the ICAR-CPCRI damage level caused by RSW, which categorized as low (<10 egg spirals per leaflet), medium (10 to 20 egg spirals per leaflet), and high (>20 egg spirals per leaflet). The observations were made from four pest infested leaflets from each coconut palms. The leaflets were randomly selected from four leaf fronds in the outer whorl situated in the four directions of the palm tree leaflets (Boopathi et al., 2017; Mohan et al., 2017; Wankhede *et al.*, 2023).

3.8 STATISTICAL ANALYSIS

The results of the field trials were analyzed statistically for validation and significance using SPSS software. The significant effect of the electrostatic charging (independent variables) on the deposition, percentage coverage and deposit density (dependent variables) were determined by ANOVA (analysis of variance). Tukey's honest significance test (Tukey-HSD) was used for the comparison of means at a confidence level of 95%. The effect of electrostatic spraying in controlling the whitefly population was determined by paired T-test.

3.9 COST ESTIMATION

The fabrication cost of the developed prototype was calculated by summing the individual costs of each component, along with machine work and labour charges. Operational costs, including both fixed and variable cost, were estimated following the methods recommended by the IS (Indian Standards) code:9164-1979.

3.9.1 Fixed cost

The fixed costs were calculated based on an assumed functional life of 5 years with an expected annual usage of 250 hours. The fixed costs included depreciation, interest, shelter and insurance for the machine.

3.9.1.1 Depreciation

Depreciation accounts the decline in the value of the initial cost over a year. The annual depreciation was determined using the following equation:

$$D = \frac{P - S}{L}$$ Equation 39

Where,

D : Depreciation cost, Average per annum

P : Purchase price of the equipment

L : Useful life of machine in years (taken as 8 years)

S : Residual value of the equipment (5 per cent of the P)

3.9.1.2 Interest

Interest on investment contributes a major portion of the fixed cost after depreciation. It is a direct expense on borrowed capital. The interest rate is taken as 12 per cent of average purchase price. Average purchase price (A) can be calculated using Equation *40*.

$$A = \frac{(P + S)}{2}$$ Equation 40

3.9.1.3 Taxes, insurance and housing

Taxes, insurance and housing cost (TIH) together is significantly lower than the depreciation and interest, but should still be taken into account. Generally, farm machinery and equipment are exempt from taxes, so this can be disregarded. Tax an insurance is calculated as 2 per cent of the average purchase price, whereas the housing is calculated on the basis of 1.5 per cent of the average purchase price.

3.10 **Variable costs**

Variable costs include expenses such as repairs and maintenance, fuel, lubrication, and labour charges incurred during the machine's operating hours.

3.10.1.1 Repair and maintenance cost

Repair and maintenance costs are one of the important aspects of machine ownership. Regular maintenance and occasional repairs are necessary to ensure the machine remains in good working condition. Factors that necessitate repairs and maintenance include routine wear and tear, accidental damage, operator negligence, and scheduled overhauls. The annual cost of repairs and maintenance (C_{RM}) is estimated to be 5 per cent of the machine's initial cost.

3.10.1.2 Cost of battery recharging

The annual cost of recharging a lead-acid battery (sealed, maintenance-free, with a 4-year lifespan) can be calculated using the formula below. This calculation considers the electrical energy consumed based on the battery's discharged capacity, the cost of electricity, and the number of recharging cycles per year.

$$C_{RC} = E_{RC} \times N_{RC} \times E_{UC} \qquad \text{Equation 41}$$

Where,

C_{RC} : Annual battery recharging cost, Rs. per annum

N_{RC} : Number of recharging cycles per annum, Nos

E_{UC} : Per unit cost of electricity, Rs. per kWh

E_{RC} : Consumption of electrical energy for each recharge cycle, kWh

And, E_{RC} could be calculated using the following equation:

$$E_{RC} = \frac{V_b \times A_b \times (100 - B_C) \times (100 + B_L)}{10^7} \qquad \text{Equation 42}$$

Where,

V_b : Open circuit voltage of battery, V

A_b : Capacity of battery, Ah

B_C : Battery charge potential when discharged, 20 per cent

B_L : Charging losses, 20 per cent

3.10.1.3 Labour cost

The labour cost for operating the machine can be determined based on the current labour rates in Tavanur, Kerala, calculated as Rs. per day for 8 working hours. An average agricultural labour rate of Rs. 750 per day was used for this calculation. The total hourly operating costs of sprayers were calculated by dividing the combined fixed and variable costs by the sprayer's annual working hours.

$$Total\ Operationl\ Cost, Rs.h^{-1} = \frac{Fixed\ costs + variable\ costs}{Annual\ working\ hours}$$

Equation 43